Colloids and Surfaces B: Biointerfaces 88 (2011) 181–190

Contents lists available at ScienceDirect

Colloids and Surfaces B: Biointerfaces

journal homepage: www.elsevier.com/locate/colsurfb

Modulation of cyanobacterial photosystem I deposition properties on alkanethiolate Au substrate by various experimental conditions

Dibyendu Mukherjee[a,b], Michael Vaughn[a,c,1], Bamin Khomami[a,b], Barry D. Bruce[a,b,c,*]

[a] Sustainable Energy Education and Research Center (SEERC), University of Tennessee, Knoxville, TN 37996, USA
[b] Department of Chemical and Biomolecular Engineering, University of Tennessee, Knoxville, TN 37996, USA
[c] Department of Biochemistry, Cellular and Molecular Biology, University of Tennessee, Knoxville, TN 37996, USA

ARTICLE INFO

Article history:
Received 21 February 2011
Received in revised form 22 June 2011
Accepted 22 June 2011
Available online 19 July 2011

Keywords:
AFM
Photovoltaics
SAM
Photosystem I
Trimeric and monomeric complex
Directionality

ABSTRACT

We present results from atomic force microscopy (AFM) images indicating various experimental conditions, which alter the morphological characteristics of self-assembled cyanobacterial PS I on hydroxyl-terminated self-assembled alkanethiolate monolayers (SAM/Au) substrates. AFM topographical images of SAM/Au substrates incubated in solutions containing different PS I concentrations solubilized with Triton X-100 as the detergent reveal large columnar aggregates (~100 nm and hence, much taller than a single PS I trimer) at high PS I concentrations. Depositions from dilute PS I suspensions reveal fewer aggregates and relatively uniform surface topography (~10 nm). Confocal fluorescence microscopy analysis of fluorescently tagged PS I deposited on to SAM/Au substrates using electric field and gravity driven techniques reveal preliminary indications of directionally aligned PS I attachments, besides corroborating a uniform monolayer formation [1], for the former deposition method. The complex attachment dynamics of PS I onto SAM substrates are further investigated from the AFM images of PS I/SAM/Au substrates prepared under different experimental conditions using: 1) PS I isolated as monomers and trimers 2) adsorption at elevated temperatures, and 3) different detergents with varying pH values. In each of the cases, the surface topology indicated distinct yet complex morphological and phase characteristics. These observations provide useful insight into the use of experimental parameters to alter the morphological assembly of PS I on to SAM substrates *en route* to successful fabrication of PS I based biohybrid photoelectrochemical devices.

1. Introduction

The current worldwide energy usage is ~15 TW (1 TW = 10^{12} W) [2] and has been projected to reach ~28 TW by year 2050 and 43 TW by year 2100 [3]. Although the earth receives ~120,000 TW of solar energy in a highly distributed and very reliable fashion, current direct photovoltaic conversion accounts for a meager <0.1% of the worldwide energy usage while dwindling natural gas, coal and petroleum reserves supply >80% of the energy requirements [2,8]. This increasing demand in global energy and availability of abundant solar energy has generated a tremendous interest in using natural and/or artificial photosynthesis as a sustainable and alternative energy sources [4–7]. Nature has evolved a photosynthetic mechanism that plants, algae and cyanobacteria use to harness solar energy with very high internal quantum efficiency. The central process of photosynthetic energy conversion involves reaction centers that both capture the light energy and convert it into a stable charge separation. In oxygenic photosynthesis two reaction centers, Photosystem II and Photosystem I, work in series to oxidize water and reduce NADP+. Photosystem I (PS I), a supra-molecular protein complex (MW ~ 300 kDa) that acts like a nano-scale biological photodiode, is a crucial component for driving this natural photosynthesis mechanism [8–10]. Upon exposure to light, PS I undergoes charge separation and creates a reducing potential across photosynthetic membranes which in turn enables unidirectional electron flow. This effectively functions like a natural photovoltaic (PV) structure. Recent advances in nanobiotechnology using the photo-activated electron transport of PS I to directly generate hydrogen [11–15] and a detailed understanding of the structural and dimensional characteristics of PS I from crystallographic studies [9,16,17] have encouraged researchers to consider using the photo-induced electrochemical activities of PS I to fabricate future bio-hybrid photovoltaic devices. Critical constraints lie in extracting these proteins from their natural

* Corresponding author at: Barry. D Bruce, 226 Hesler Biology Bldg., Biochemistry, Cellular and Molecular Biology, 125 Austin Peay Bldg., University of Tennessee at Knoxville, Knoxville, TN 37996, USA. Tel.: +1 011 865 974 4082; fax: +1 011 865 974 6306.
E-mail address: bbruce@utk.edu (B.D. Bruce).
[1] Present address: Department of Chemistry and Biochemistry, Arizona State University, Tempe, AZ 85287, USA.

0927-7765/$ – see front matter © 2011 Elsevier B.V. All rights reserved.
doi:10.1016/j.colsurfb.2011.06.029

thylakoid membranes and encapsulating them in organic/inorganic substrates as a first step towards PV device fabrication. Surface immobilization of these proteins through self-assembly mechanisms is an obvious yet elegant approach. Furthermore, this immediately calls for a clear understanding of the surface attachment dynamics and controlling the properties of these protein complexes on a self-assembled monolayer (SAM) [1]. As part of our ongoing research to tap the potential of PS I as a biomaterial for future photovoltaic devices, our goal in this work is to analyze the different surface morphological characteristics of PS I attained when adsorbed onto alkanethiolate SAM/Au substrates under different experimental conditions.

In general, numerous studies extensively investigated the various applications and limitations of the interfacial chemistry and surface engineering to monitor protein adsorption on solid and polymeric surfaces [18–20]. Other studies have researched the effect of varying the surface hydrophilicity on the interfacial energetics of protein adsorption onto polymeric surfaces [21]. Diffusion driven aggregation dynamics of bovine serum albumin (BSA) proteins on PEG (polyethylene glycol) SAMs have been previously reported [22], whereas adsorption dynamics of BSA on gold surfaces have been studied in detail using dynamic contact angle (DCA) and quartz-crystal microbalance (QCM) measurements [23].

One of the earliest works reporting PS I assembly on gold surfaces for photovoltaic applications used chemical platinization of PS I to facilitate PS I welding to Au via PS I-Pt–Au bonding affinity [24]. The mechanism for such chemical "welding" is not very well-understood and makes such methods far more complex raising serious concerns with regards to the repeatability and uniformity of this technique. Numerous recent reports have resorted to simpler self-assembly techniques, thereby elucidating various methods and characteristics of PS I adsorption onto alkanethiolate self-assembled monolayer (SAM) on Au surfaces [25,26]. Amongst some of the notable previous investigations studying dependence of PS I immobilization on various substrate properties, Ciobanu et al. [27] have reported the first directed adsorption of PS I by using patterned surfaces decorated with chemically altered sites that enhanced or hindered the protein adsorption. This enabled them to achieve site-specific attachment of the protein complex that was analyzed with the aid of scanning electrochemical microscopy (SECM). Additionally, related reports include monolayer assemblies of various light harvesting core complexes [28] from photosynthetic bacteria on alkanethiolate gold or amino-terminated indium tin oxide (ITO) electrodes

In an effort to further demonstrate the applications of photosynthetic protein complexes for various bio-derived photoelectrochemical devices, research has also been directed in establishing the electrostatic potential on single reaction centers [29] and photoelectrochemistry of their monolayer substrates [30]. Such efforts pave the way for various recent studies [31] highlighting the photovoltaic activity of PS I-SAM systems such as fabrication of various photo-electronic devices by direct chemical binding of PS I to gold surface via surface engineered cysteine residues [32], and bio-hybrid solid-state electro-optical devices by electronic coupling between photosynthetic reaction centers and semiconducting materials [33]. In recent years, significant research has focused on integration of photosynthetic protein complexes (*e.g.* bacterial reaction centers, PS I and PS II) assembled on to various SAM/Au substrates in the fabrication of solid-state electronic devices [34] and biosensors [35,36].

The vast amount of literature dedicated towards the application of PS I and PS II for photovoltaic, bio-electronic and photo-electrochemical applications is highly encouraging for the sustainable energy research community to increasingly integrate biological systems and components into novel energy solutions. Yet, the bottleneck in converting these small-scale proof-of-concept efforts into functioning PV devices, suitable for engineering research interests, remains at the critical fabrication step. We must be able to reliably and repeatedly produce uniform monolayer deposition of these proteins on an organic/inorganic interface. Currently, the lack of information on the adsorption characteristics of PS I particles from detergent solubilized solutions onto typical SAM/Au substrates have left most researchers working with PS I/SAM/Au systems for photovoltaic applications with minimal validation of monolayer formation. In the past, in an effort to incorporate PS I into various materials, earlier work has also shown that these proteins attach themselves favorably onto OH-terminated thiols without denaturation [25,26,30]. Also, one of the earliest reports [37] claims that surfaces carrying OH-terminated thiols allow directional adsorption of PS I with 70% of their electron-transfer vectors pointing outward. Although such studies provide us with valuable information for interfacing PS I with various organic/inorganic substrates, none of them carry out any detailed study of the characteristic properties of the surface attachment dynamics of these proteins on SAM.

In an effort to acquire a better understanding of the factors controlling the morphology of surface immobilized PS I on alkanethiolate SAM/Au substrates, the present study extends our recent efforts [1] on understanding the roles of self and directed assembly of PS I to adsorptions carried out under various experimental conditions such as: 1) adsorption temperature; 2) use of trimeric or monomeric form of the PS I complex; 3) use of different detergents in aqueous buffer solutions with various pH levels during the self-assembly process and finally, 4) use of fluorescently tagged PS I trimeric complexes to compare the attachment characteristics under self (gravity-driven) and directed (electric field assisted) assembly techniques. Our results indicate that self-assembly of PS I adsorbed onto SAM/Au substrates lead to complex morphological arrangements that may be experimentally controlled as described below.

2. Materials and methods

2.1. Growth of Thermosynechococcus elongatus and preparation of Photosystem I

The thermophilic cyanobacterium *T. elongatus* BP-1 was grown in 2 L airlift fermenters (Bethesda Research Labs, Bethesda MD) in NTA media [38]. The temperature was held at 56 °C with continuous illumination by fluorescent lights. The light level was increased as the cultures approached higher densities to a maximum of 50 $\mu E/m^2/s$. Cells were collected during late log phase by centrifugation for 10 min at 7000 *g*, and washed once in wash buffer, 20 mM MES pH 6.5, 5 mM $MgCl_2$, and 5 mM $CaCl_2$ before storage at −20 °C until use for PS I preparation. Frozen cells were resuspended in 20 mM MES pH 6.5, 5 mM $MgCl_2$, 5 mM $CaCl_2$ and 500 mM sorbitol. The resuspended cells were adjusted to a chl *a* content of 1 mg/mL [39] and homogenized using a Dounce homogenizer. Lysozyme was added to 0.2% (w/v) and the mixture was incubated for 2 h at 37 °C with shaking. The resulting mixture was centrifuged as before and the supernatant was discarded. The pellet was resuspended in the wash buffer. Again the volume was adjusted so that the chl *a* concentration was 1 mg/mL; the mixture was then lysed in a French press at 20,000 psi twice. The highly fluorescent lysate was centrifuged at 20,000 rpm in a Sorvall centrifuge with a SS-34 rotor for 20 min, and the supernatant was discarded. The crude membrane fragments collected in the pellet were washed once with a wash buffer containing 3 M NaBr then twice in the initial wash buffer. The final washed membrane fragments were adjusted to a chl *a* concentration of 1 mg/mL and *n*-dodecyl-β-D maltoside (DM) was added to a final concentration of 0.6% w/v and the mixture was incubated

for 20 min at 20 °C in darkness with gentle stirring. The insoluble material was removed from the solubilized membrane mixture by centrifugation in the SS-34 at 20,000 rpm (~50,000 g) for 30 min. The supernatant was separated immediately from the pellet and then loaded onto 10–30% (w/v) sucrose gradients with 60% (w/v) cushion; all solutions in the gradient also contained 20 mM MES and 0.03% DM. Density gradient centrifugation was performed at 24,000 rpm in an SW28 rotor at 10 °C for 16 h. The lowest green band contained the trimeric PS I complex; these bands were collected and pooled using a large syringe. Pooled PS I samples were slowly diluted five-fold by addition of MES pH 6.5 with 0.03% DM (w/v), and then loaded onto a POROS 20HQ (Applied Biosystems) anion exchange column and eluted with $MgSO_4$ in a minimal volume. Finally the $MgSO_4$ was removed by dialyzing against 20 mM MES pH 6.5, 500 μM C_aCl_2, 500 μM $MgCl_2$, and 0.03% DM, and based on spectrophotometer measured chl *a* concentrations, PS I concentration in the buffer solution was estimated to be around $C_B = 1.42 \times 10^{-5}$ mol/L. Purified and extracted PS I samples were stored in aliquots of 1.5 mL at -80 °C for future use.

2.2. Preparation of alkanethiolate SAM/Au substrates

Commercial Au coated Si wafers (Au layer thickness ~10 nm, Platypus Technologies) were dipped in freshly prepared Aqua Regia (concentrated HCl and HNO_3 acids in volumetric ratio of 3:1 respectively) prior to adsorbing thiols onto the surface. Freshly cleaved Au substrates (Au thickness ~60–70 nm) were then immersed in 1 mM ethanolic solution of 11-mercapto-1-undecanol ($HS–C_{11}H_{22}–OH$, 97%, Sigma–Aldrich) overnight (24–36 h) at room temperature in a chamber filled with inert dry N_2. Thiolated Au substrates were washed in isopropanol (Electronic grade residue free; 99%), deionized water, and finally dried under a stream of dry N_2. Monolayer formation was confirmed by measuring the thiol thickness on Au substrates at multiple spots using spectroscopic ellipsometer and was determined to be ~1.0 nm.

2.3. PS I deposition on the alkanethiolate SAM/Au substrates

The alkanethiolate SAM/Au substrates were immersed in different concentrations of PS I prepared by diluting concentrated PS I samples with $C_B = 1.42 \times 10^{-5}$ mol/L (as prepared in section 2.1 earlier) in 200 mM Na-Phosphate aqueous buffer solutions with pH 7.0. All buffer solutions were contained 0.02% v/v Triton X-100 as the detergent (Anagrade, Anatrace Inc., Maumee, OH) for bulk suspension of PS I. Specifically for the study of using different detergents, a 0.05% w/v of *n*-Dodecyl-β-D-maltoside (DM) made from 1% w/v aqueous solutions and prepared from powdered samples (Glycon Biochemicals, Luckenwalde, Germany) was used as the detergent for PS I suspension in 200 mM Na-phosphate aqueous buffer solutions with two different pH values of pH 6.0 and 7.0. For all the cases studied here, excluding the electric field assisted depositions, surface attachment was accomplished via self-assembled deposition on thiolated Au surfaces with an incubation time of 5 min.

For the temperature study, PS I trimers are surface immobilized by immersing the SAM/Au substrates into the bath of 200 mM Na-Phosphate aqueous buffer solution of PS I (pH 7.0; 0.02% w/v Triton X-100) at different temperatures. The PS I solutions prepared in glass beakers were suspended in a water bath whose temperature was monitored by a digital thermocouple.

Electric field assisted depositions were carried out by using the standard Novex (X-Cell SureLock Mini-Cell) blotting plate electrodes (details as shown in Fig. 1) connected to a stable constant voltage electrophoresis power source (Bio-Rad) operated at an applied voltage of 2 V for 5 min. This generated the desired electric field across the aqueous buffer solution of PS I entrapped as the dielectric medium between the electrodes. Based on observations from earlier work [1,29], the target alkanethiolate SAM / Au substrate is mounted on the anodic plate (negative electrode).

2.4. Confocal fluorescence microscopy to test site-specific PS I attachment

For both gravity and electric field assisted deposition, experiments were particularly designed to test the site-specific attachments of PS I on OH-terminated alkanethiols (11-mercapto-1-undecanol) using confocal fluorescence microscopy (Leica TCS-NT) to detect the fluorescently tagged PS I on SAM/Au substrates. Immunofluorescent detection of PS I carried out using two rabbit polyclonal primary antibodies specifically raised against cyanobacterial psaD and psaE subunits (kindly provided by Dr. John Golbeck, Penn. State University) both located on the stromal (top) side of PS I. The primary antibodies (denoted 1°) were in turn specifically tagged with commercially provided donkey anti-rabbit secondary antibodies (denoted 2°) labeled with Alexa 546 fluorochrome (Molecular Probes) and excited at 556 nm.

Freshly cleaved commercial Au coated Si wafers (as described above) of 2.6 cm × 2.6 cm size were surface treated as shown in Fig. 2A. The wafer was first half-immersed in thiol, using the same procedure described in Section 2.3 above, to create the SAM on the bottom-half, while the top half was exposed to an alkaline wash with an aqueous solution of $NH_4OH:H_2O_2:H_2O$ (3:1:40) to ensure a complete removal of any excess thiol. The complete wafer was washed in deionized water and dried in dry N_2 stream. Subsequently it was treated with 1% w/v of bovine serum albumin (Albumin, Fraction V; United States Biochemical) in phosphate buffer solutions (PBS) to block the non-specific areas devoid of proteins. This was followed by either gravity-driven or electric field assisted deposition of PS I from aqueous buffer solution of 3.6×10^{-5} mM (i.e., 400× dilutions) resulting in both specific (on thiolated areas) and some non-specific (on non-thiolated areas) attachments. The left half of the wafer (created by turning the wafer counter-clockwise by 90°) was then exposed simultaneously to both 1° antibodies. Finally, the complete wafer was exposed to the fluorophore labeled 2° antibodies. With this method, 4 different labeling combinations were created on the substrate: 1) thiolated Au with specifically attached PS I tagged by both 1° and 2° antibodies (bottom-left quadrant); 2) thiolated Au with attached PS I labeled non-specifically by the 2° antibodies alone (bottom-right quadrant); 3) non-thiolated Au surface with both non-specifically attached PS I and non-specifically tagged by the 2° antibodies (top-right quadrant) and 4) non-thiolated Au with few non-specifically attached PS I specifically tagged by both 1° and 2° antibodies (top-left quadrant). The 4 quadrants, thus obtained and labeled as BL, BR, TR and TL respectively in Fig. 2A, should ideally result in strong fluorescent signals from the BL quadrant, along with relatively weaker signals from the BR and TL quadrant and extremely weak / no signals from the TR quadrant to establish the specific/ non-specific attachments of PS I on the treated substrates.

2.5. Atomic force microscopy (AFM)

All surface topography images were collected on an Asylum Research Inc. atomic force microscopy (AFM) instrument (Model: MFP-3D-BIO) in the tapping mode using a 34 N/m silicon nitride tip with a resonant frequency of 300 kHz.

2.6. Molecular modeling and dipole moment calculation

The electrostatic surface potential of trimeric PS I has been estimated using the protein portion of the structure (PDB ID: 1JB0). The calculations were performed using CHARMM [40] and

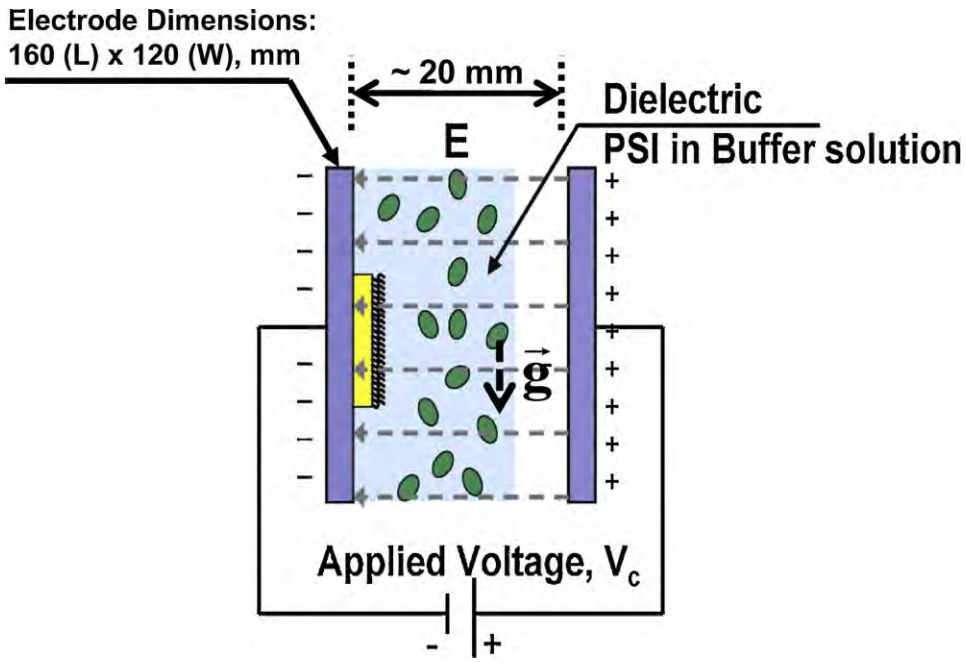

Fig. 1. Schematic showing the arrangement and dimensions of *Novex* make gel electrophoresis plate electrodes used for electric field assisted assembly of photosystem I (PS I) on SAM/Au substrates.

the CHARMM-GUI interface [41] for numerical solutions to the Poisson–Boltzmann equation [42]. This value was calculated at a neutral pH with an ionic strength of 150 mM. As is shown in Fig. 6A, the potential of the lumenal surface is primarily negative, while the stromal face shown in Fig. 6B is largely positive. The isopotential surfaces of +1 kcal/mol e^- and −1 kcal/mol e^- are represented in with the color blue and red, respectively. The sum of these charges results in a strong dipole (seen in Fig. 6C) which is indicated for each monomer as the smaller yellow arrows, while the sum of the three monomer dipoles associated with a single trimer is represented by the large arrow is orthogonal to the membrane plane due to the C_3 axis of symmetry in the trimeric arrangement. The component vectors are indicated from the geometric center of each monomer while the summed vector is positioned so its center passes through the geometric center of the trimer. The dipole vectors are drawn in the convention of a negative base, with the tip pointing in the positive direction.

3. Results and discussions

3.1. Verification of site-specific and directional attachment characteristics of PS I

Immunofluorescently detected PS I immobilized on site-specifically patterned SAM/Au substrates, as described earlier in experimental Section 2.4 and shown in Fig. 2A, clearly exhibited strong fluorescent signals from PS I undergoing site-specific attachment on the thiol activated zones of the substrate (i.e., BL quadrant of the substrate in Figs. 2B and C) along with weaker signals from the rest of the quadrants when excited and viewed under confocal fluorescence microscopy. Specifically, for both gravity driven and electric field assisted deposition techniques, Fig. 2D shows that the maximum integrated fluorescent signal intensity is emitted from the ALEXA-detected PS I immobilized in the BL quadrant area of the substrate, thereby indicating that the OH-terminated alkanethiolate areas promote directional attachment of a large number of PS I complexes with their stromal side up since immunofluroescent detection was specific to psaD and psaE subunits located on the stromal side of PS I. Apart from this, weak integrated signals from the BR and TL quadrants along with minimal intensities from TR quadrant as seen in Fig. 2D for gravity and electric field assisted depositions reveal weak non-specific attachments of either PS I or fluorophores.

Added to this, we note significantly larger integrated fluorescence intensity from the activated BL quadrant for electric field assisted deposition as compared to the corresponding signal from gravity driven deposition. Based on preliminary semi-quantitative computational modeling using only the protein fragments of PS I from the trimeric crystal structure (discussed earlier in Section 2.6), the estimated effective dipole moment vector (Fig. 6C) of PS I points in the positive direction away from the lumenal (bottom) side of the trimer. This suggests that under applied electric field, the PS I trimeric complex along with its net positive charge distribution [29] (Figs. 6A–C) should align itself with the anodic plate. This prediction is corroborated by experimental observations that a large number of PS I complexes, while undergoing deposition on the anodic surface [1], possibly directionally align themselves with the fluorophore labeled antibodies on the stromal psaD and psaE subunits facing up, thereby enabling a higher immunofluorescent detection of PS I. More definitively, it is noted that a higher exposure of the fluorophores on the stromal psaD and psaE subunits enabling an enhanced fluorescent signal (Fig. 2D; refer to the schematic in Fig. 2E) suggests the formation of uniform PS I monolayer. This observation also concurs with our recent studies on electric filed assisted deposition of PS I on to SAM substrates [1] indicating that the interactions of the applied electric field with the inherent dipole moment of PS I trimers (refer to Fig. 6C) facilitates in disrupting the aggregates formed in the solution. Such observations offer a preliminary indication that under externally applied field, PS I undergoes a more uniform and directionally aligned attachments as compared to the gravity driven case. In the absence of an external field non-uniform and agglomerated PS I arrangements prevent formation of a uniform monolayer, which will be a subject of extensive discussion in the subsequent sections. For clarity, these treatments have been schematically illustrated in Fig. 2E.

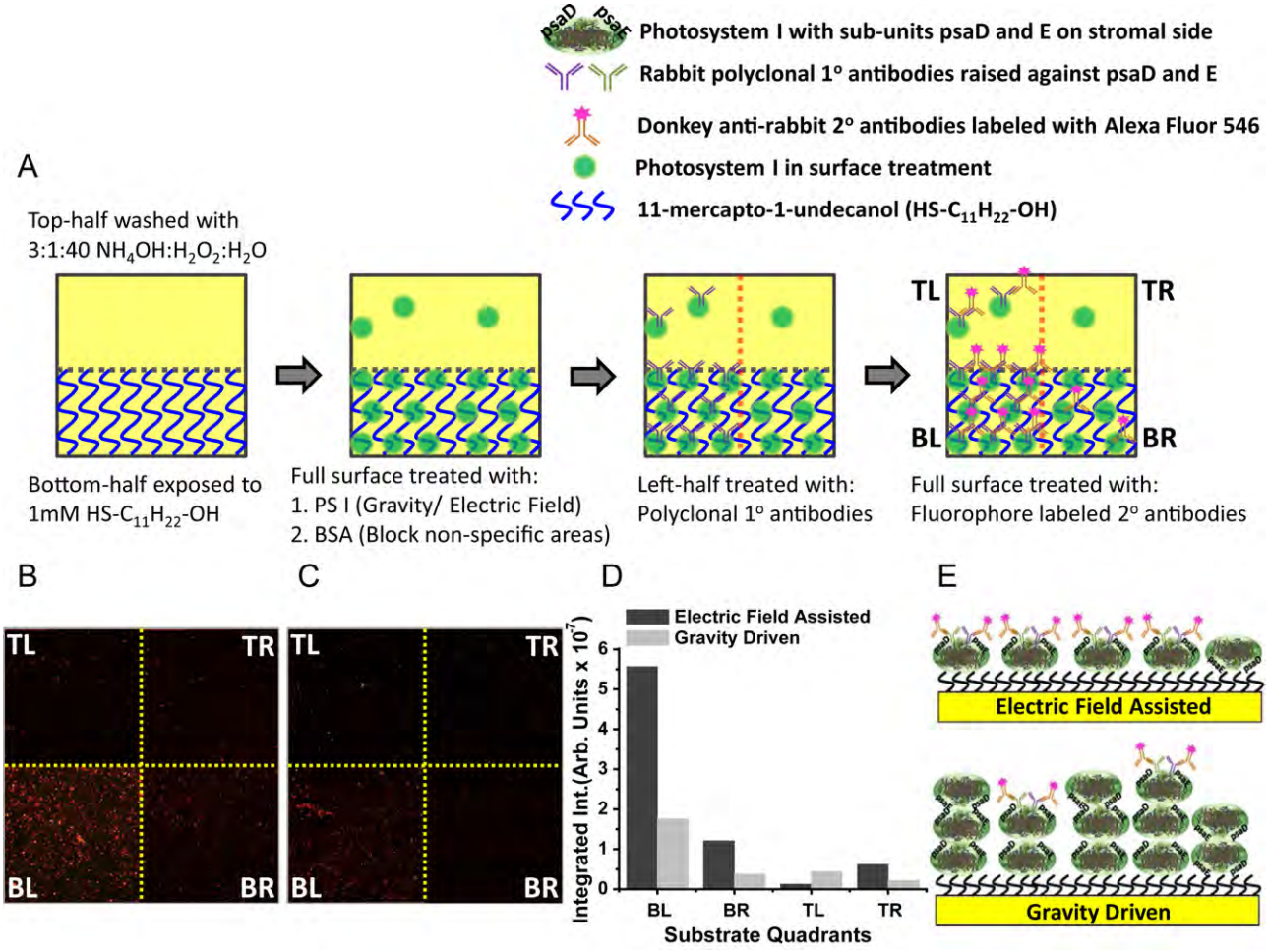

Fig. 2. (A) Schematic showing the fabrication of patterned SAM/Au substrates with 4 quadrants (BL, BR, TL and TR) created to test the site-specific attachments of fluorescently labeled PS Is deposited using both gravity and electric fields assisted techniques (descried in details in Section 2.4); confocal microscopy images of the fluorescence detected in the 4 quadrants (labeled as BL, BR, TL and TR) from the Alexa Fluor 546 labeled PS Is deposited via (B) electric-field assisted and (C) gravity driven techniques; (D) Net fluorescence signal intensities as obtained from the 4 substrate quadrants (BL, BR, TL and TR) for both electric-field assisted and gravity driven depositions; (E) Schematics explaining the variations in signal intensities as a result of the accessibility of fluorophore tagged antibodies to psaD and psaE sub-units of PS I due to their possible arrangements on SAM/Au substrates arising out of electric-field assisted and gravity driven deposition techniques.

3.2. Adsorption characteristics for different PS I concentrations in buffer

Surface topography AFM images recorded for gravity driven surface immobilization from different PS I concentrations (described in the earlier section) have been shown in Fig. 3A–C. These images indicate that at higher concentrations, as also observed from our earlier studies [1], the protein complexes tend to aggregate thereby adsorbing as clusters onto the SAM/Au substrate whereas as the concentration lowers the clusters dissipate into more uniform layers of PS I adsorption. We notice that depositions from higher PS I concentration of 7.2×10^{-5} mM (200× dilutions) result in columnar clusters whose heights are of the order of ~100 nm as indicated by the scale of the AFM image in Fig. 3A. Also, these structures are not uniformly distributed and tend to have a large distribution of sizes on the surface. Upon further dilution i.e. PS I concentration of 3.6×10^{-5} mM (400× dilution), the depositions show a disruption of the columnar structures although the PS I adsorptions still form large crusts of multiple layers (~20–30 nm) as seen from the scale of Fig. 3B. In comparison to this, deposition from extremely low PS I concentration of 1.8×10^{-5} mM (800× dilution) result in a complete breakdown of the larger structures, thereby indicating a uniform, homogeneous layer of PS I trimers (thickness ~10 nm) dispersed more evenly across the substrate (Fig. 3C).

This can be explained by the fact that high protein concentrations promote large scale aggregation due to enhanced protein–protein interactions in the solution phase. Added to this, the effective inherent dipole moment of the PS I trimer pointing from the lumenal (negative) towards the stromal (positive) side (see Fig. 6C), favors the PS I complexes to undergo the top–bottom alignments resulting in streamer like clusters that rapidly settle onto the substrate due to gravity. On the other hand, lower PS I concentration results in weaker protein–protein interactions, thereby significantly reducing the possibilities of aggregation and hence resulting in relatively uniform adsorbed layers. The aforementioned phenomenon has been extensively studied and presented in great details in our recent work [1].

3.3. Adsorption characteristics at different immobilization temperatures

In the second stage of experiments, PS I trimers are immobilized onto SAM/Au substrates at different temperatures as described earlier in Section 2.3. Based on the results from our earlier section, we used the lowest PS I concentration of 1.8×10^{-5} mM (800×) in buffer to minimize the solution phase aggregations. The experiments are run with 4 different bath temperatures of 10 °C, 22 °C, 40 °C, and 60 °C. Our results indicate that the protein complexes

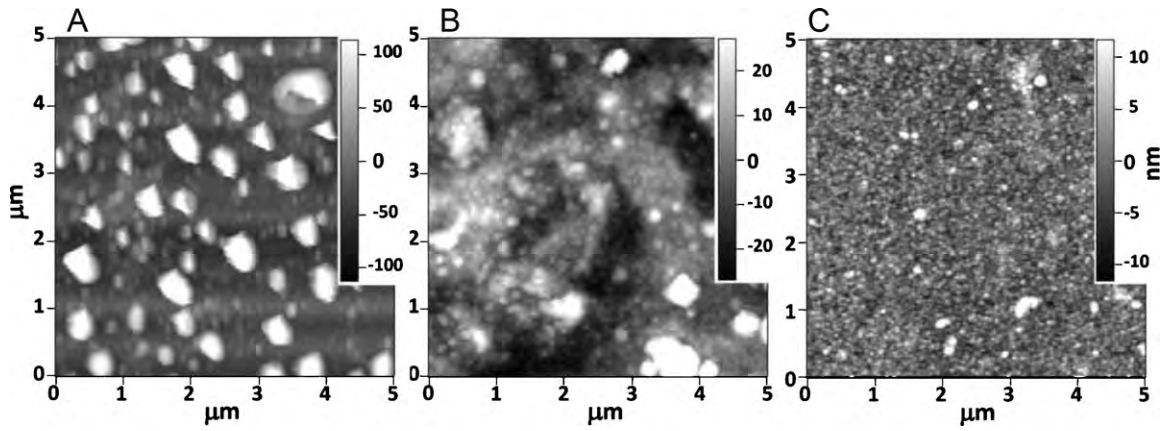

Fig. 3. Surface topology from AFM images scanned over PS I/SAM/Au substrates prepared from surface adsorption of PS I from different concentrations of (A) 7.2×10^{-5} mM (200×); (B) 3.6×10^{-5} mM (400×) and (C) 1.8×10^{-5} mM (800×) prepared from a base concentration of $C_B = 1.427 \times 10^{-5}$ mol/L (x being the dilution factor in each case) in 200 mM Na-Phosphate buffer solution, 0.02% w/v Triton X-100. AFM images collected with a tip of spring constant ~ 34 N/m in tapping mode.

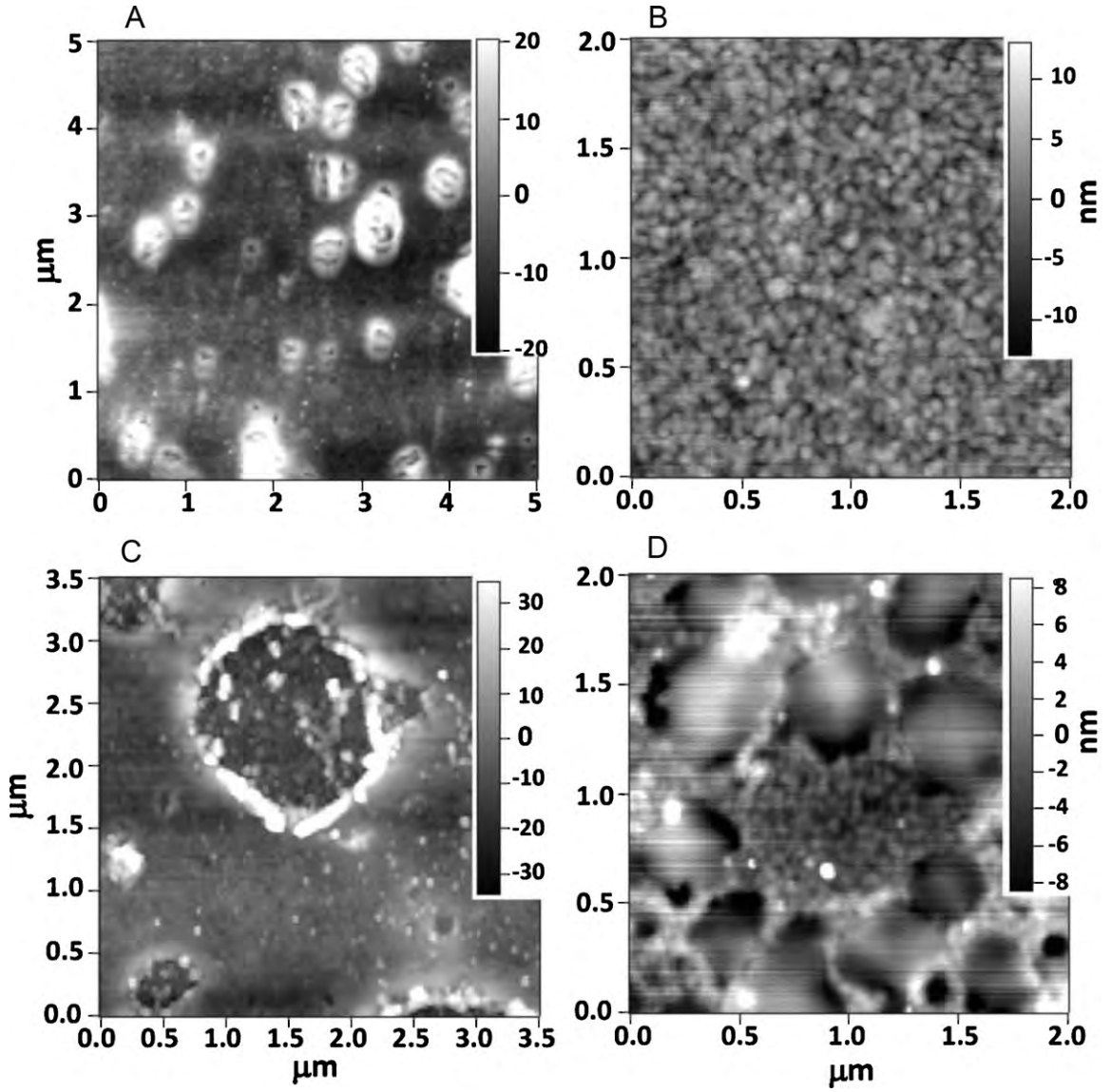

Fig. 4. Typical AFM images indicating surface topographical characteristics of PS I adsorbed from 200 mM Na-Phosphate buffer suspension (pH 7.0, 0.02% w/w Triton X-100) with a PS I concentration of 1.8×10^{-5} mM (800× dilution) under different bath temperatures T_{Bath} of: (A) 10 °C; (B) 22 °C; (C) 40 °C and (D) 60 °C.

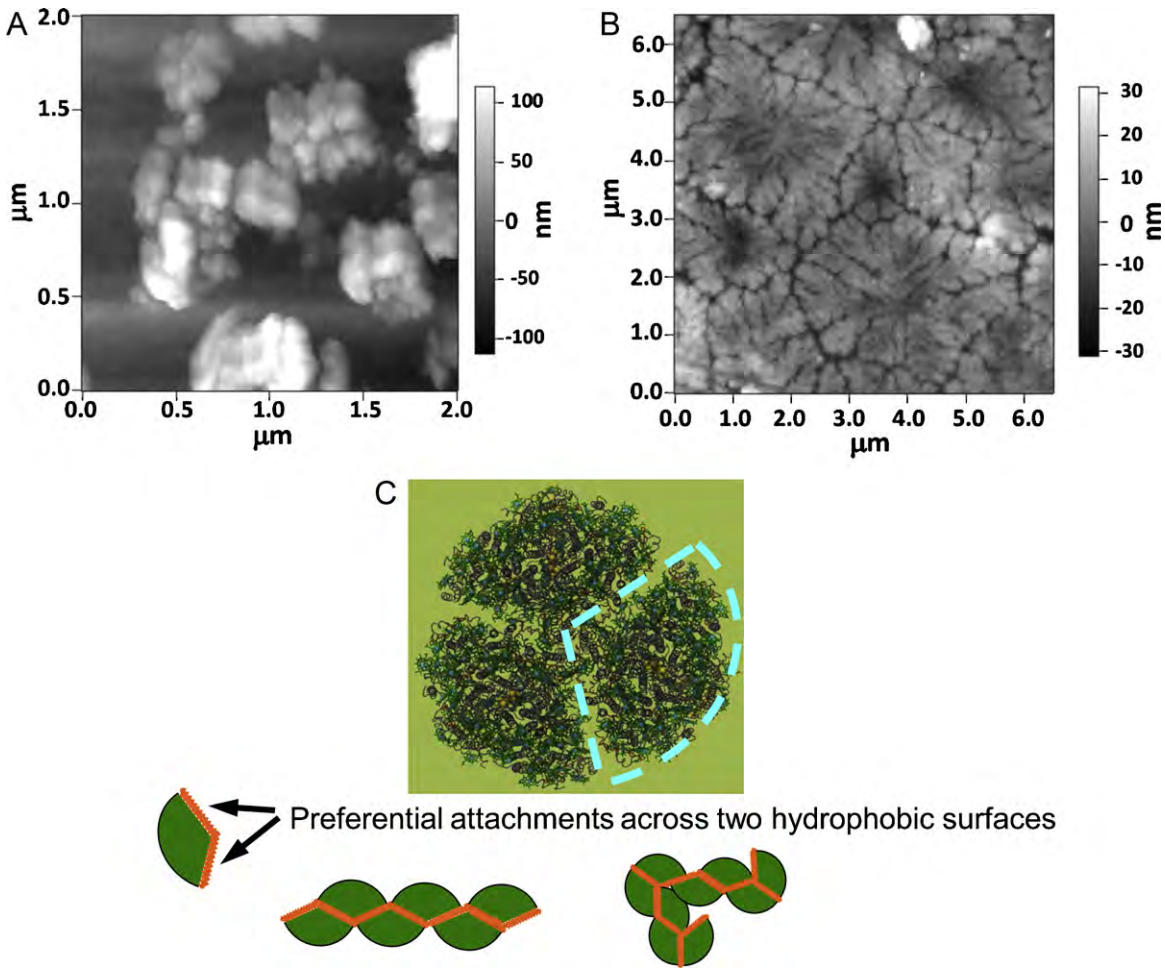

Fig. 5. (A–B) Typical AFM images for PS I monomers extracted from *Thermosynechococcus elongatus* species and adsorbed onto SAM/Au substrate from 200 mM Na-Phosphate buffer solution, 0.02% w/v Triton X-100 with PS I concentration of 3.6×10^{-8} mol/L (Dilution factor, $X = 400$). (C) Schematic representation of typical monomers extracted from the trimer configuration of PS I and its aggregation dynamics due to the two hydrophobic surfaces across each monomer that enhance preferential attachment into dendrite or fractal like structures.

can undergo severe morphological and phase transitions depending on the immobilization temperatures (see Fig. 4A–D). Thus, at 10 °C, we see that the images indicate typical concentric ring like structures that encapsulate the proteins (Fig. 4A). These structures disappeared at the room temperature, *i.e.* 22 °C, and gave way to more uniformly dispersed PS I adsorbed on the substrates as seen in Fig. 4B.

Upon raising the bath temperature to 40 °C during the surface immobilization step, PS I adsorbs onto the surface with unique features wherein the protein layers on the surface become entrapped in circular phase separated zones (Fig. 4C). A plausible explanation of this behavior is the onset of a phase separation wherein lipid membranes from the proteins separate and form the amorphous circular band, ultimately trapping the proteins inside. This also suggests the onset of denaturing of PS I, thereby indicating that temperature variations in the surface adsorption experiments are limited to temperatures where the functionality of PS I remains unaffected. Thus, finally upon raising the adsorption temperature to 60 °C, (Fig. 4D) PS I undergoes complete phase separation in which the lipid membranes forms amorphous circular patches whose boundaries distinctly separate from the bare proteins that occupy the intermediate spaces. At this temperature, PS I is potentially denatured, thereby losing its light absorbing and photoelectrochemical functionalities. The AFM images of denatured PS I at temperature ranges ~60 °C is also consistent with our recent work on PS I mediated hydrogen production [15] indicating that the photoelectrochemical activity of PS I is diminished at temperatures above 55 °C.

Cyanobacteria respond to changes in temperature by adjusting the degree of unsaturation in their fatty acids [43], and thus the phase transition behavior of their membranes is adjusted appropriately [44]. Specifically, the saturation of the galactolipid, monogalactosyl-diacylglycerol (MGDG), has been demonstrated to be regulated in response to temperature by increasing the degree of saturation [45]. Since the organism in this work is thermophilic, the fatty acids of the thylakoid lipids are largely saturated with an elevated transition temperature. Interestingly, the isolated PS I complex of *T. elongatus* has at least four tightly bound lipids as well as unresolved density between adjacent monomers that likely contain lipids [46]. Although no detailed analysis of PS I-associated detergent/lipids is available, recent work indicates that the dimeric PS II complex of *T. elongatus* is surrounded by 20 lipids and 220 detergent molecules [47]. The higher resolution crystal structure of PS II resolves 14 tightly bound lipids [48]. Of these, 13 are galactolipids, including MGDG, as well as 3 detergent molecules. All of these molecules are found at the interface of the PS II monomers. Although we do not have this level of structural insight into isolated PS I particles, its associated lipids are also likely to occupy regions at the subunit interfaces. Differential scanning calorimetry studies of MGDG isolated from a thermophilic cyanobacteria grown

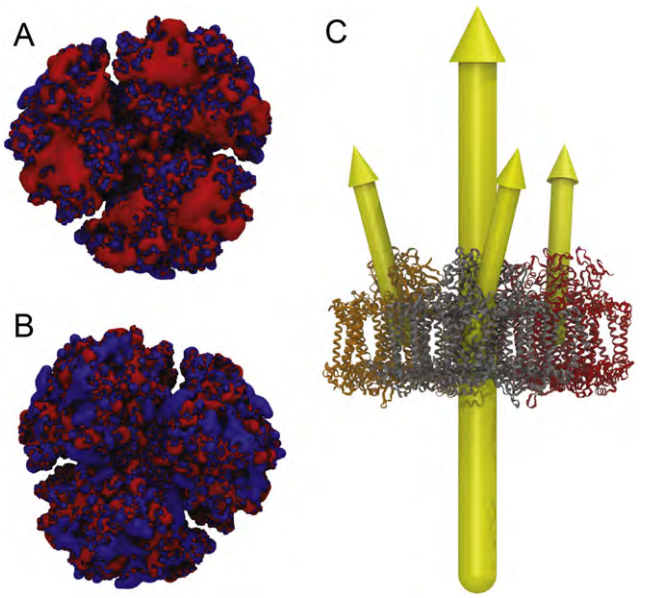

Fig. 6. (A–C) Isopotential surfaces of +1 kcal/mol e⁻ and −1 kcal/mol e⁻ represented in blue and red respectively on: (A) stromal (top) and (B) lumenal (bottom) faces of PS I trimer; (C) Schematic of the dipole moment vector as estimated from computational modeling for charge distribution within PS I trimer (described in text under Sections 2.6 and 3.5) with the small yellow arrows indicating vectors for each monomer (represented in orange, gray or red ribbons), and a large yellow arrow for the entire complex. Figure was composed using the molecular graphics software program VMD [53]. (For interpretation of the references to color in this figure legend, the reader is referred to the web version of the article.)

at 38 °C, indicate that this lipid undergoes its transition at ~38 °C [49]. When the PS I particles are adsorbed at elevated temperatures such as 40 °C and 60 °C they may be above their transition temperature and behave as a liquid crystal phase. Deposition at these temperatures may allow the lipids/detergent molecules in a liquid-crystal phase to dissociate from the PS I complex and coalesce into a bulk liquid-crystalline phase. The observation of a clear bulk phase separation following deposition at elevated temperatures suggests that lipid phase transitions of the PS I-associated lipid/detergents can modulate and influence the macroscopic organization of PS I complexes during deposition (Fig. 4A–D).

3.4. Adsorption characteristics for PS I monomeric complexes

The PS I monomers extracted as per the procedures described in Section 2 earlier were matched to a 400× dilution (i.e., 3.6×10^{-5} mM) as used in PS I trimer adsorption studies to enable elucidation of the surface morphology of PS I monomers upon gravity driven immobilization on SAM/Au substrates. Interestingly, the surface topography of PS I monomer attachments on SAM/Au substrates exhibit enhanced agglomeration resulting in bulky fractal-like structures as seen from Fig. 5A and B. This morphology may be explained by the fact that the "pie-shaped" monomer sector extracted from the original trimer arrangement of the protein, as indicated by the schematic in Fig. 5C, offers two hydrophobic surfaces across which the PS I can preferentially attach to each other. This increases the surface area available for the protein–protein interactions thereby resulting in an enhanced aggregation process that can lead to chain-like or fractal-like arrangements as demonstrated schematically in Fig. 5C.

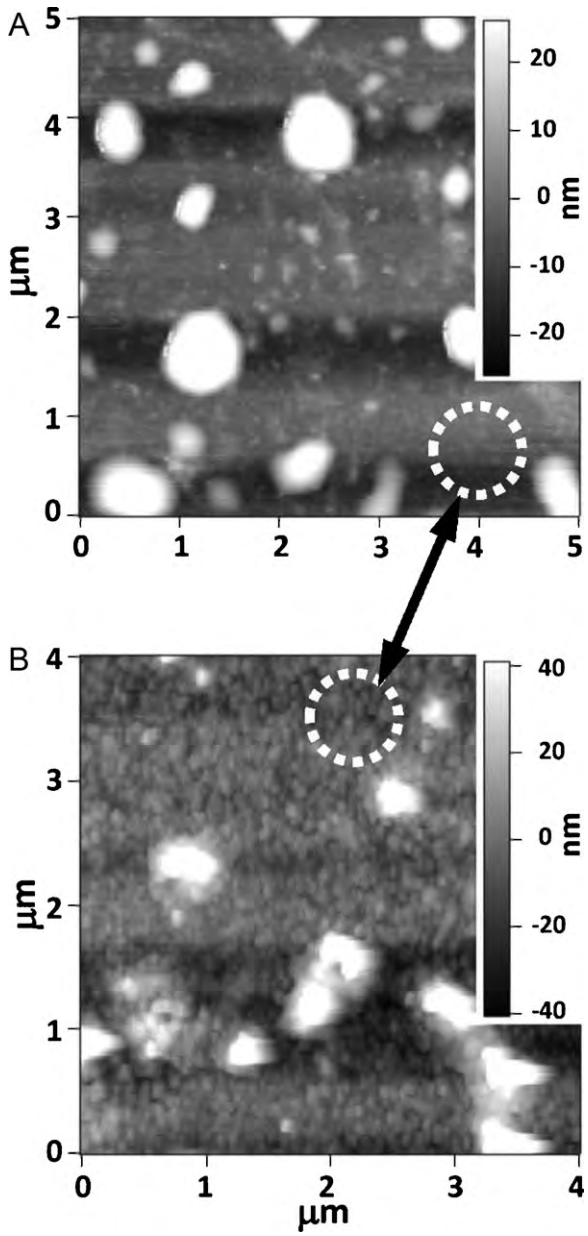

Fig. 7. AFM images of topographical arrangements of PS I adsorbed onto SAM/Au substrate from 200 mM Na-Phosphate buffer solution with 0.05% w/w DM as the detergent (PS I concentration of 3.568×10^{-8} mol/L, dilution factor of $X = 400$) and two different pH values of (A) pH 6.0 and (B) pH 7.0 to show the role of detergents in the aggregation dynamics of PS I. The marked areas indicate the distribution of PS I in the intermediate areas between the columnar structures deposited on the SAM/Au substrates.

3.5. Adsorption characteristics for PS I suspended with DM as detergent

Finally, PS I deposition onto SAM/Au substrates were carried out from the aqueous buffer solution of PS I with DM as the detergent (details regarding the concentration is described in details in materials and methods section) to further investigate the role of buffer mediated solution phase protein-protein interaction in driving PS I aggregation dynamics on the surfaces. The experimental conditions chosen were 200 mM Na-Phosphate buffer solutions with two different pH values of 6.0 and 7.0 (Fig. 7A). Our AFM results indicate that the surface topology show similar patterns of large columnar aggregated structures for the case of PS I deposition from a DM based buffer solution with pH of 6.0. However,

the PS I deposition from buffer with pH 7.0 and a concentration of 3.6×10^{-5} mM (dilution factor, $X = 400$) created more uniform layers with less aggregated protein masses on the substrate as clearly seen from Fig. 7B. It should be noted that previous studies have also observed that the secondary structures of PS I are more prone to denaturation when stabilized with Triton X-100 as the detergent [50]. Additionally, micelle size and concentration of Triton X-100 and DM may affect protein-detergent interactions, thereby altering the aggregation dynamics of PS I in solution phase, which in turn affects the surface attachment dynamics. Our on-going studies have indicated a strong correlation between the relative concentrations of PS I complexes/detergent used to prepare the colloidal buffer suspension and the aggregation behavior of PS I in solution phase which has been exclusively studied elsewhere [51] for a detailed understanding of the phenomenon.

Also, in Fig. 7A and B the indicated areas demonstrate the uniformity of PS I deposition in between the aggregated columnar structures. There is no evidence of PS I deposition on the substrate surfaces surrounding the columnar structures at the lower pH (Fig. 7A) implying that the majority of the PS I complexes have arranged themselves into the aggregated structures. In comparison to this, Fig. 7B shows large number of individual protein complexes distributed uniformly over large areas of the substrate thereby proving the decreased affinity to self-assemble into columnar aggregates even at the same dilution range ($X = 400$) for which we had noticed substantially increased aggregation in our earlier case studies (Fig. 3B) with Triton X-100 as the detergent.

4. Conclusion

The results presented here demonstrate that while OH-terminated thiols facilitate the preferential adsorption of PS I from buffer solutions onto the SAM/Au substrates, the topographical morphology of PS I is controlled by various experimental parameters and deposition dynamics, i.e., bulk aggregation in self-assembly depositions or external electric-field mediated disruption of the aggregates via interactions with inherent PS I dipole moment [1]. At high concentrations enhanced protein–protein interactions, facilitated by the inherent dipole moment of the PS I trimers, promote their top-bottom alignments forming clusters that eventually sediment out on the substrates as large columnar aggregates. In the lower concentration cases, weaker protein–protein interactions result in smaller sized PS I clusters to deposit onto the substrates, thereby resulting in nearly uniform PS I monolayers. Immunofluorescent detection of PS I trimers adsorbed on to SAM/Au substrates using electric field assisted deposition, when compared to the ones from gravity driven depositions, provide preliminary proofs for their directional attachments. Our results qualitatively suggest that, under external electric field, PS I trimers preferentially attach with the lumenal surface on the anodic electrode. Such an alignment is in agreement with our preliminary structure based semi-quantitative computational modeling for the PS I dipole moment and charge distribution.

Furthermore, PS I isolated from the thermophilic cyanobacterium *T. elongatus* carry a significant complement of the native membrane lipids, which form different temperature-dependent phases, thereby generating various surface topographies when deposited under different ambient temperatures. Deposition at >40 °C results in the onset of the separation of lipid membranes from the protein complexes, whereas for temperatures ≥60 °C, PS I undergoes complete phase separation from the lipid membranes resulting in possible denaturing of the protein and hence breakdown of its photo-electrochemical properties. However previous studies indicate that detergent solubilized PS I is functional at these temperatures [52], thus further investigation is required. Experiments run by replacing Triton X-100 with DM as the detergent in buffer solutions containing identical concentrations of PS I with a pH of 7.0 indicated reduced aggregations and hence, more uniform depositions. Although for the lower pH of 6.0 we observe a higher degree of aggregation similar to the Triton X-100 case study.

Acknowledgements

This work was funded by Sustainable Energy Education and Research Center (SEERC) at UTK to B.D.B. and B.K. This work was also supported by a National Science Foundation (NSF) Nanoscience Interdisciplinary Research Team (NIRT) award to B.D.B. (DBI-0403781). Additional support was provided to B.D.B, B.K. and D.M. from the Gibson Family Foundation. We would like to acknowledge Dr. John Dunlap with the Microscopy Center at UTK for his help and guidance with the AFM images.

References

[1] D. Mukherjee, M. May, M. Vaughn, B.D. Bruce, B. Khomami, Controlling the morphology of photosystem I assembly on thiol-activated Au substrates , Langmuir 26 (2010) 16048–16054.
[2] R.E. Blankenship, D.M. Tiede, J. Barber, G.W. Brudvig, G. Fleming, M. Ghirardi, M.R. Gunner, W. Junge, D.M. Kramer, A. Melis, T.A. Moore, C.C. Moser, D.G. Nocera, A.J. Nozik, D.R. Ort, W.W. Parson, R.C. Prince, R.T. Sayre, Comparing photosynthetic and photovoltaic efficiencies and recognizing the potential for improvement , Science 332 (2011) 805–809.
[3] N.S. Lewis, D.G. Nocera, Powering the planet: chemical challenges in solar energy utilization , Proc. Natl. Acad. Sci. USA 103 (2006) 15729–15735.
[4] A. Listorti, J. Durrant, J. Barber, Artificial photosynthesis: solar to fuel , Nat. Mater. 8 (2009) 929–930.
[5] J. Barber, Photosynthetic energy conversion: natural and artificial , Chem. Soc. Rev. 38 (2009) 185–196.
[6] M. Hambourger, G.F. Moore, D.M. Kramer, D. Gust, A.L. Moore, T.A. Moore, Biology and technology for photochemical fuel production , Chem. Soc. Rev. 38 (2009) 25–35.
[7] D. Gust, T.A. Moore, A.L. Moore, Solar fuels via artificial photosynthesis , Acc. Chem. Res. 42 (2009) 1890–1898.
[8] D.A. LaVan, J.N. Cha, Approaches for biological and biomimetic energy conversion , Proc. Natl. Acad. Sci. USA 103 (2006) 5251–5255.
[9] P. Jordan, P. Fromme, H.T. Witt, O. Klukas, W. Saenger, N. Krauss, Three-dimensional structure of cyanobacterial photosystem I at 2.5 angstrom resolution , Nature 411 (2001) 909–917.
[10] N. Nelson, Plant photosystem I—the most efficient nano-photochemical machine , J. Nanosci. Nanotechnol. 9 (2009) 1709–1713.
[11] J.F. Millsaps, B.D. Bruce, J.W. Lee, E. Greenbaum, Nanoscale photosynthesis: photocatalytic production of hydrogen by platinized photosystem I reaction centers , Photochem. Photobiol. 73 (2001) 630–635.
[12] B.R. Evans, H.M. O'Neill, S.A. Hutchens, B.D. Bruce, E. Greenbaum, Enhanced photocatalytic hydrogen evolution by covalent attachment of plastocyanin to photosystem I , Nano Lett. 4 (2004) 1815–1819.
[13] C.E. Lubner, P. Knorzer, P.J.N. Silva, K.A. Vincent, T. Happe, D.A. Bryant, J.H. Golbeck, Wiring an [FeFe]-hydrogenase with photosystem I for light-induced hydrogen production , Biochemistry 49 (2010) 10264–10266.
[14] C.E. Lubner, R. Grimme, D.A. Bryant, J.H. Golbeck, Wiring photosystem I for direct solar hydrogen production , Biochemistry 49 (2010) 404–414.
[15] I.J. Iwuchukwu, M. Vaughn, N. Myers, H. O'Neill, P. Frymier, B.D. Bruce, Self-organized photosynthetic nanoparticle for cell-free hydrogen production , Nat. Nano 5 (2010) 73–79.
[16] I. Grotjohann, P. Fromme, Structure of cyanobacterial photosystem I , Photosynth. Res. 85 (2005) 51–72.
[17] A. Amunts, H. Toporik, A. Borovikova, N. Nelson, Structure determination and improved model of plant photosystem I , J. Biol. Chem. 285 (2010) 3478–3486.
[18] V. Hlady, J. Buijs, Protein adsorption on solid surfaces , Curr. Opin. Biotechnol. 7 (1996) 72–77.
[19] N. Nath, J. Hyun, H. Ma, A. Chilkoti, Surface engineering strategies for control of protein and cell interactions , Surf. Sci. 570 (2004) 98–110.
[20] P.A. Underwood, J.G. Steele, Practical limitations of estimation of protein adsorption to polymer surfaces , J. Immunol. Methods 142 (1991) 83–94.
[21] P. Cha, A. Krishnan, V.F. Fiore, E.A. Vogler, Interfacial energetics of protein adsorption from aqueous buffer to surfaces with varying hydrophilicity , Langmuir 24 (2008) 2553–2563.
[22] Z. Yang, J.A. Galloway, H. Yu, Protein interactions with poly(ethylene glycol) self-assembled monolayers on glass substrates: diffusion and adsorption , Langmuir 15 (1999) 8405–8411.
[23] H. Stadler, M. Mondon, C. Ziegler, Protein adsorption on surfaces: dynamic contact-angle (DCA) and quartz-crystal microbalance (QCM) measurements , Anal. Bioanal. Chem. 375 (2003) 53–61.

[24] J.W. Lee, I. Lee, E. Greenbaum, Platinization: A novel technique to anchor photosystem I reaction centres onto a metal surface at biological temperature and pH , Biosens. Bioelectron. 11 (1996) 375–387.
[25] B.S. Ko, B. Babcock, G.K. Jennings, S.G. Tilden, R.R. Peterson, D. Cliffel, E. Greenbaum, Effect of surface composition on the adsorption of photosystem I onto alkanethiolate self-assembled monolayers on gold , Langmuir 20 (2004) 4033–4038.
[26] H.A. Kincaid, T. Niedringhaus, M. Ciobanu, D.E. Cliffel, G.K. Jennings, Entrapment of photosystem I within self-assembled films , Langmuir 22 (2006) 8114–8120.
[27] M. Ciobanu, H.A. Kincaid, G.K. Jennings, D.E. Cliffel, Photosystem I patterning imaged by scanning electrochemical microscopy , Langmuir 21 (2005) 692–698.
[28] M. Kondo, Y. Nakamura, K. Fujii, M. Nagata, Y. Suemori, T. Dewa, K. Lida, A.T. Gardiner, R.J. Cogdell, M. Nango, Self-assembled monolayer of light-harvesting core complexes from photosynthetic bacteria on a gold electrode modified with alkanethiols , Biomacromolecules 8 (2007) 2457–2463.
[29] I. Lee, J.W. Lee, A. Stubna, E. Greenbaum, Measurement of electrostatic potentials above oriented single photosynthetic reaction centers , J. Phys. Chem. B 104 (2000) 2439–2443.
[30] M. Ciobanu, H.A. Kincaid, V. Lo, A.D. Dukes, G.K. Jennings, D.E. Cliffel, Electrochemistry and photoelectrochemistry of photosystem I adsorbed on hydroxyl-terminated monolayers , J. Electroanal. Chem. 599 (2007) 72–78.
[31] I. Carmeli, L. Frolov, C. Carmeli, S. Richter, Photovoltaic activity of photosystem I-based self-assembled monolayer , J. Am. Chem. Soc. 129 (2007) 12352–12353.
[32] L. Frolov, Y. Rosenwaks, C. Carmeli, I. Carmeli, Fabrication of a photoelectronic device by direct chemical binding of the photosynthetic reaction center protein to metal surfaces , Adv. Mater. 17 (2005) 2434.
[33] L. Frolov, Y. Rosenwaks, S. Richter, C. Carmeli, I. Carmeli, Photoelectric junctions between GaAs and photosynthetic reaction center protein , J. Phys. Chem. C 112 (2008) 13426–13430.
[34] R. Das, P.J. Kiley, M. Segal, J. Norville, A.A. Yu, L.Y. Wang, S.A. Trammell, L.E. Reddick, R. Kumar, F. Stellacci, N. Lebedev, J. Schnur, B.D. Bruce, S.G. Zhang, M. Baldo, Integration of photosynthetic protein molecular complexes in solid-state electronic devices , Nano Lett. 4 (2004) 1079–1083.
[35] J. Maly, J. Krejci, M. Ilie, L. Jakubka, J. Masojidek, R. Pilloton, K. Sameh, P. Steffan, Z. Stryhal, M. Sugiura, Monolayers of photosystem II on gold electrodes with enhanced sensor response—effect of porosity and protein layer arrangement , Anal. Bioanal. Chem. 381 (2005) 1558–1567.
[36] J. Maly, J. Masojidek, A. Masci, M. Ilie, E. Cianci, V. Foglietti, W. Vastarella, R. Pilloton, Direct mediatorless electron transport between the monolayer of photosystem II and poly (mercapto-p-benzoquinone) modified gold electrode-new design of biosensor for herbicide detection , Biosens. Bioelectron. 21 (2005) 923–932.
[37] I. Lee, J.W. Lee, E. Greenbaum, Biomolecular electronics: vectorial arrays of photosynthetic reaction centers , Phys. Rev. Lett. 79 (1997) 3294–3297.
[38] J.F. Tailing, D. Driver, in: M. Doty (Ed.), Primary Productivity Measurement, Marine and Fresh-water, U.S. Atomic Energy Commission, Washington, D.C, 1963, p. 142.
[39] J.F. Talling, D. Driver, Some problems in the estimation of chlorophyll a in phytoplankton , in: M. Doty (Ed.), Primary productivity measurement, marine and freshwater, Vol TID 7633, US Atomic Energy Commission, Washington, DC, 1963.
[40] B.R. Brooks, R.E. Bruccoleri, B.D. Olafson, D.J. States, S. Swaminathan, M. Karplus, Charmm—a program for macromolecular energy, minimization, and dynamics calculations , J. Comput. Chem. 4 (1983) 187–217.
[41] W. Im, D. Beglov, B. Roux, Continuum solvation model: computation of electrostatic forces from numerical solutions to the Poisson–Boltzmann equation , Comput. Phys. Commun. 111 (1998) 59–75.
[42] S. Jo, M. Vargyas, J. Vasko-Szedlar, B. Roux, W. Im, PBEQ-solver for online visualization of electrostatic potential of biomolecules , Nucl. Acids Res. 36 (2008) W270–W275.
[43] N. Sato, N. Murata, Y. Miura, N. Ueta, Effect of growth temperature on lipid and fatty acid compositions in the blue-green algae, *Anabaena variabilis* and *Anacystis nidulans* , Biochim. Biophys. Acta 572 (1979) 19–28.
[44] N. Murata, Low-temperature effects on cyanobacterial membranes , J. Bioenerg. Biomembr. 21 (1989) 61–75.
[45] N. Sato, N. Murata, Temperature shift-induced responses in lipids in the blue-green alga, *Anabaena variabilis*: the central role of diacylmonogalactosylglycerol in thermo-adaptation , Biochim. Biophys. Acta 619 (1980) 353–366.
[46] P. Fromme, P. Jordan, N. Krauss, Structure of photosystem I , Biochim. Biophys. Acta 1507 (2001) 5–31.
[47] J. Kern, B. Loll, C. Luneberg, D. DiFiore, J. Biesiadka, K.D. Irrgang, A. Zouni, Purification, characterisation and crystallisation of photosystem II from *Thermosynechococcus elongatus* cultivated in a new type of photobioreactor , Biochim. Biophys. Acta 1706 (2005) 147–157.
[48] B. Loll, J. Kern, W. Saenger, A. Zouni, J. Biesiadka, Lipids in photosystem II: interactions with protein and cofactors , Biochim. Biophys. Acta 1767 (2007) 509–519.
[49] D.A. Mannock, A.P.R. Brain, W.P. Williams, Phase-behavior of the membrane-lipids of the thermophilic blue-green-alga *Anacystis nidulans* , Biochim. Biophys. Acta 821 (1985) 153–164.
[50] X. Ruan, J. Wei, Q. Xu, J.-s. Wang, Y.-d. Gong, X.-f. Zhang, T.-y. Kuang, N.-m. Zhao, Comparison of the effects of Triton X-100 treatment on the protein secondary structure of photosystem I and photosystem II studied by FT-IR spectroscopy , J. Mol. Struct. 525 (2000) 97–106.
[51] D. Mukherjee, M. May, B. Khomami, Detergent-protein interactions in aqueous buffer suspensions of Photosystem I (PS I) , Journal of Colloid and Interface Science 358 (2) (2011) 477–484.
[52] I.J. Iwuchukwu, M. Vaughn, N. Myers, H. O'Neill, P. Frymier, B.D. Bruce, Self-organized photosynthetic nanoparticle for cell-free hydrogen production , Nat. Nanotechnol. 5 (2010) 73–79.
[53] W. Humphrey, A. Dalke, K. Schulten, VMD: visual molecular dynamics , J Mol Graphics 14 (1996) 33-&.